

Magnetic phase diagram for FeCO_3 , an Ising antiferromagnet with anti-ferromagnetic inter- and intrasublattice exchange coupling

V. V. Eremenko, N. F. Kharchenko, L. I. Belyi, M. Gillaud¹⁾, A. Marshan¹⁾, and P. Feldman²⁾

Low Temperature Physicotechnical Institute, Academy of Sciences, Ukrainian SSR

(Submitted 11 May 1985)

Zh. Eksp. Teor. Fiz. **89**, 1712–1733 (November 1985)

The behavior of the two-sublattice collinear antiferromagnetic material FeCO_3 in strong pulsed or dc magnetic fields $\mathbf{H} \parallel C_3$ is investigated by magneto-optical and magnetic techniques. Comparison of the results of the pulsed and static experiments indicates that the antiferromagnet FeCO_3 is strongly cooled by magnetizing pulses of amplitude close to the magnetic transition field H_1 . The magnetic phase diagram in the H, T plane is found, and it is shown that FeCO_3 exists in a mixed magnetic state for fields $H_1 < H < H_2$ and temperatures below the critical point $T_c \approx 4$ K; this state can be described in terms of a restructuring of soliton lattices in the field. It is shown that FeCO_3 belongs to a little-studied class of Ising antiferromagnets in which magnetic ions in both identical and different sublattices are involved in antiferromagnetic exchange interactions.

1. INTRODUCTION

Iron carbonate, which occurs naturally as siderite, is a familiar example of a two-sublattice collinear antiferromagnetic (AFM) material with easy-axis anisotropy. Although the impurities in naturally occurring minerals vary qualitatively in composition and concentration from one sample to another, the properties of optically transparent siderite crystals are well-defined, and the onset of magnetic ordering occurs at temperatures close to the Néel temperature $T = 38$ K for synthetic FeCO_3 powder.

The rhombohedral calcite structure of the FeCO_3 crystals does not change upon oxidation. The magnetic and chemical unit cells coincide and are described by the $R\bar{3}C$ magnetic space group.¹ The magnetic moments of the Fe^{2+} ions are directed along the C_3 trigonal axis. The crystals contain alternating layers in which the Fe^{2+} spins point “up” and “down,” respectively. The low-energy spectrum of FeCO_3 is accurately described by the two-sublattice Ising model, which is valid because the closest excited energy lies quite far from the ground-state Kramers doublet.² The nearest neighbors of each Fe^{2+} ion belong to the second sublattice and are arranged in two adjacent layers; they are coupled by the exchange interaction to the central AFM Fe^{2+} ion. There is no consensus regarding the nature of the interaction among the ions that lie in the second coordination sphere, belong to the same sublattice, and are contained in a single layer. Model interactions involving only nearest neighbors have been used to explain the observed far-IR absorption,^{3,4} Raman scattering,^{5,6} inelastic neutron scattering,^{7–9} and Mössbauer effect.^{10–12} The temperature dependence of the sublattice magnetization,⁹ the available data on the temperature dependence of the magnetic susceptibility,^{13,14} the observation of a sharp transition from the AFM to the saturated paramagnetic (PM) states in a magnetic field,^{15,16} and an analysis of the possible exchange couplings¹⁵ all suggest that the interaction between second magnetic neighbors is ferromagnetic in nature.^{3,9,15–17} At first glance, this conclusion would appear to be supported by the

marked hysteresis in the magnetic properties during the phase transition. However, unlike other Ising antiferromagnets in which both the inter- and the intralattice interactions are antiferromagnetic (e.g., as in the classical metamagnets such as FeCl_2 (Ref. 18)), the transition in FeCO_3 from the AFM to the saturated paramagnetic state is gradual rather than abrupt and occurs over a wide range of magnetic fields $H_1 < H < H_2$ of width > 30 kOe. This interval exceeds the maximum interval $4\pi\Delta M = 9$ kOe determined by the demagnetizing fields.

Careful measurements of the differential magnetic susceptibility in experiments with pulsed magnetic fields have revealed that the transition has a magnetic fine structure—there are two small but abrupt changes in the magnetization at the endpoints H_1, H_2 of the field interval, within which the susceptibility χ oscillates with a small magnitude.^{19–21} There is a rapid increase in the hysteresis when H approaches H_2 . It was noted in these papers that the magnetization in siderite behaves much like that in type-II superconductors, and a model was proposed in which the Fe^{2+} ions belonging to the same sublattice are antiferromagnetically coupled. The smoothness of the AFM→PM transition was attributed to a quasicontinuous change in the number of magnetic sublattices and to the formation of a superstructure of period much greater than the dimensions of the chemical elementary cell.

In the molecular field approximation, the simple two-sublattice model of Ising antiferromagnets with AFM intralattice exchange predicts that there is a range of fields within which neither the AFM nor the PM states are stable at $T = 0$ K (Ref. 22). This difficulty can be eliminated by considering additional sublattices. The problem was analyzed in Ref. 23 for a cubic antiferromagnet with four sublattices, and it was found that when the temperature drops below $T_c = (a_{nnn}J_{nnn}/z_{nn}J_{nn})T$, the AFM→PM transition may occur as a series of phase transitions, one of which is first-order (here J_{nn} and J_{nnn} are the exchange interactions for nearest [z_{nn}] and second-nearest [z_{nnn}] neighbors). However, studies of the AFM→PM phase transition temperature for FeCO_3 in pulsed fields²⁴ give a critical temperature

$T_c = (0.7-0.8)T$, which is too high. Indeed, this value of T_c would require that the interactions J_{nn} and J_{nnn} be similar in strength, which is hardly likely for FeCO_3 . Moreover, the interval H_2-H_1 would also have to be much wider than is actually observed.

The experimentally observed hysteresis of FeCO_3 during pulsed magnetization also lacks a clear-cut explanation. Although the hysteresis makes it obvious that the AFM \rightarrow PM transition must be nonequilibrium, the reason for the nonequilibrium nature of the transition has not been resolved. Various mechanisms have been proposed^{16,21,25,26} to account for the hysteresis for fields extending down to $H = 0$, but none of them gives a unified, self-consistent treatment of the magnetic phase transition in siderite.

The conflicting interpretations of the magnetic transition in FeCO_3 are primarily the result of difficulties in ascertaining the magnetic phase composition of the crystals for $H_1 < H < H_2$ and to the lack of data on the degree of (thermodynamic) equilibrium of the transition process. Experiments in dc fields and magneto-optical studies of small regions of siderite crystals could be particularly informative here, and such experiments were carried out in our present work. We measured the magnetization $M(H)$ and susceptibility χ in dc fields, and the magneto-optical (Faraday) rotation $\Phi(H)$ of the polarization plane of light in pulsed fields. Surprisingly, our results on $M(H)$ in static fields did not suffice to establish the qualitative nature of the magnetic phase transition in FeCO_3 . Although $M(H)$ and $\Phi(H)$ recorded in pulsed fields^{19-21,27} have pronounced peaks at H_1 and H_2 , we did not observe such peaks for $M(H)$ recorded in static fields even for $T = 1.5$ K. On the other hand, the width $\Delta H = H_2 - H_1$ of the AFM \rightarrow PM transition interval was comparable to that for the pulsed measurements. Comparison of the pulsed and quasistatic results revealed that FeCO_3 undergoes substantial cooling during magnetization in a pulsed field. This adiabatic cooling turns out to be of crucial importance for reconstructing the phase diagram of FeCO_3 from pulsed data. Measurements of the differential susceptibility in quasistatic fields for T below 4 K demonstrated that two phase transitions occur at the endpoints H_1, H_2 for sufficiently low temperatures. The magneto-optical studies showed that the phase of the sample was homogeneous for almost all H in (H_1, H_2) , except in the immediate vicinity of H_2 . Our results suggest that the phase transition at H_1 is second-order and remains so for T down to ~ 0.5 K. Finally, we used the experimental data to plot the magnetic phase (HT) diagram for FeCO_3 and determined the critical temperature $T_c = 6 \pm 2$ K (this value is consistent with the magnitude and AFM nature of the exchange interaction among the second-nearest neighbors as estimated from the fields H_1 and H_2). The rest of this paper is concerned with a discussion of these results.

2. EXPERIMENTAL METHODS

Most of the experiments discussed here were carried out at the Low Temperature Physicotechnical Institute, Academy of Sciences, Ukrainian SSSR (pulsed magneto-optical measurements) and at the L. Néel Laboratory, National

Center for Scientific Research, France (dc measurements). Identical siderite specimens obtained from Greenland deposits were studied. The magneto-optical studies were carried out in the longitudinal Faraday geometry $\mathbf{k} \parallel \mathbf{H} \parallel C_3$. The Faraday rotation in FeCO_3 reaches $46 \text{ deg/cm} \cdot \text{kOe}$ for $T \approx T_N$ and is $\approx 1.5 \cdot 10^4 \text{ deg/cm}$ near magnetic saturation; it can thus be measured without difficulty by straightforward techniques. We used two beams and a Wollaston prism analyzer to decrease the errors caused by mechanical vibrations of the crystal during a field pulse. The alignment of the crystal was monitored by analyzing conoscopic patterns, and \mathbf{k} and \mathbf{H} were parallel to C_3 to within 1 and 3 degrees, respectively (these misalignments did not materially contribute to the experimental error). There were no cold windows in the optical channel, and the crystal was mounted on a cooled heat exchanger. The rise time of the field pulse was varied from $1.5 \cdot 10^{-3}$ to $3.5 \cdot 10^{-3}$ s, and the amplitude ranged up to 350 kOe. We measured the time dependence of the current through the solenoid by using a specially designed low-inductance resistor²⁸; the phase of the voltage across the resistor was precisely matched with the current and magnetic field strength in the solenoid. We calibrated the solenoid and verified that the voltage drop along the resistor was proportional to the field strength (and that the voltage and field phases were equal) by measuring the Faraday rotation in fused quartz. An He-Ne laser of wavelength 6328 \AA served as the light source.

The dc measurements were carried out in a solenoid capable of generating magnetic fields up to 180 kOe. The magnetic measurements were carried out using a vibration magnetometer.

3. EXPERIMENTAL RESULTS AND DISCUSSION

3.1 Relation between the Faraday rotation and the magnetization of siderite

In order to quantitatively compare the magnetic and magneto-optical properties, one must first determine the extent to which the paramagnetic Faraday rotation Φ is directly proportional to the magnetization M . Because the crystal field causes extensive mixing of the multiplet states in compounds containing elements in the Fe group, the proportionality coefficient $K = M/\Phi$ should depend on both T and H (Ref. 29). However, in FeCO_3 the magnitude of the Fe^{2+} orbital momentum that is not frozen in is nearly the same for all of the low-lying Kramers doublets, and the nearest level for which the orbital momentum is different lies at an energy of $\approx 10^3 \text{ cm}^{-1}$. We therefore anticipated that K would be constant up to high temperatures $T \gg T_N$. For low temperatures $T < 70$ K, for which only the lowest Kramers doublet is populated, the conditions for K to be constant are even more favorable. Because state mixing caused by the magnetic field must be of minor importance even in strong fields because the energy levels are widely separated and the Fe^{2+} ligand environment is highly symmetric, we expected that K would be constant for all experimental fields, provided the frequency of the optical probing beam remained well away from the frequencies of the electron transitions contributing appreciably to the rotation.

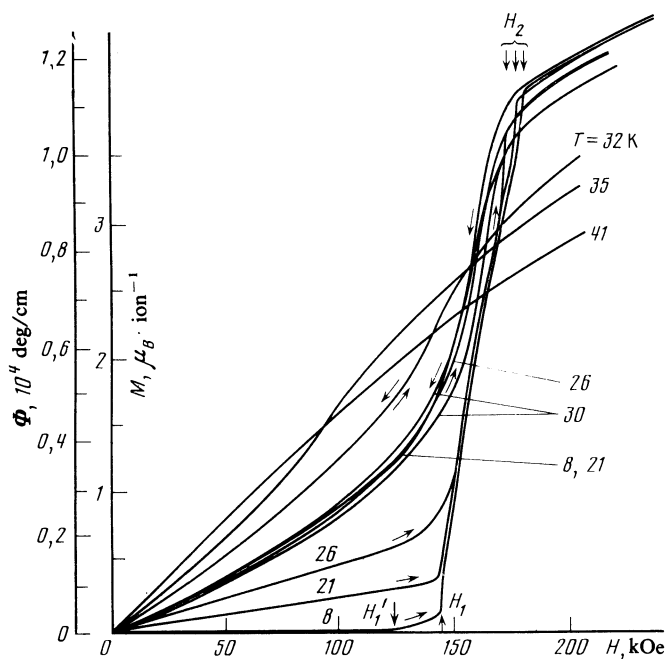


FIG. 1. Faraday rotation and magnetization of siderite ($M \propto \Phi$) as a function of the strength of the pulsed magnetic field for several initial sample temperatures.

We tested these conclusions by measuring the wavelength and temperature dependences of the Faraday rotation. The influence of intraconfiguration transitions near $\lambda = 6328 \text{ \AA}$ was too small to be measured. We compared the temperature dependence $\rho(T)$ of the specific rotation with available data on $\chi(T)$ presented in Ref. 13 for several siderite specimens and found that $\rho(T)$ and $\chi(T)$ become directly proportional at temperatures above T_N , while for $T < T_N$ the proportionality broke down and the curves $\rho(T)$ and $\chi(T)$ for different samples were only qualitatively similar. However, when we measured the susceptibility and compared it with the specific rotation, we found that χ and ρ were proportional even for $T < T_N$, and this continued down to 10 K. The deviations from proportionality for $T < 10 \text{ K}$ could have been due to systematic errors in the various experiments; more probably, however, they reflected the presence of impurity ions in the siderite which influenced χ and ρ to different degrees. Indeed, Mn^{2+} is usually the dominant impurity in siderite; Mn^{2+} gives a negligible contribution to the Faraday rotation but may alter χ significantly because of its large magnetic moment. In this case, the Faraday rotation should reflect the behavior of the Fe^{2+} ions more closely than the magnetization. In addition, the relative contribution of the thermal diamagnetic Faraday rotation increases as T drops, and this could also tend to make $\rho(T)$ nonproportional to $\chi(T)$. In strong fields for which the magnetization M increases much faster than H , the contribution from the diamagnetic rotation is negligible and we expect M and ρ to be proportional. Indeed, the proportionality coefficient $K = \rho(T)/\chi(T)$ deduced from the temperature curves for ρ and χ was equal to $2810 \pm 100 \text{ (deg/cm)(}\mu_B/\text{ion)}^{-1}$, which is close to the value found by comparing the Faraday rotation and the magnetization for siderite in pulsed fields

$> H_1$, the lower bound of the field interval for the magnetic transition. For example, Jacobs' data¹⁸ for $M(H)$ yield $K = \Phi(200 \text{ kOe})/M(200 \text{ kOe}) = 2820 \text{ (deg/cm)(}\mu_B/\text{ion)}^{-1}$. We will henceforth use the value $K = 2810 \text{ (deg/cm)(}\mu_B/\text{ion)}^{-1}$.

3.2 Cooling of siderite crystals during pulsed magnetization in a field $H \parallel C_3$

If we compare $M(H)$ for static fields with $M(H)$ deduced for pulsed fields from the Faraday rotation angles Φ for the same siderite sample, we conclude that the FeCO_3 crystal is substantially cooled in a pulsed field. The curves $M(H_{\text{pulse}}) = K^{-1}\Phi(H_{\text{pulse}})$ and $M(H_{\text{dc}})$ are shown in Figs. 1 and 2. The temperatures indicated in Fig. 1 are the initial temperatures T_i of the crystal at the start of the field pulse. The marked difference in the dc and pulsed curves can be explained only if the sample temperature is assumed to change greatly during pulsed magnetization. We can find these temperature changes by comparing $M(T)_{H_{\text{dc}}}$ and $M(T)_{H_{\text{pulse}}} = K^{-1}\Phi(T)_{H_{\text{pulse}}}$. The final temperatures T_f of the crystal were found by matching the values $M_{H_{\text{dc}}}$ and $M_{H_{\text{pulse}}}$ as shown in Fig. 3; the results are plotted in Fig. 4 as a function of the field strength and initial temperature. The curves in Fig. 4a correspond to constant entropy, because in fields $H < H_1$ the magnetization of siderite is an equilibrium process, as may be seen by comparing $\Phi(H)$ recorded on the leading and trailing edges of a field pulse of amplitude $H_a < H_1$. Figure 4 shows that when H_a becomes comparable to $H_1 \approx 145 \text{ kOe}$, a crystal initially at $T_i = 20 \text{ K}$ is cooled adiabatically down to 2 K, while T_f is 0.5 K or even lower for $T_i = 8 \text{ K}$. These large coolings during pulsed magnetization clearly cannot be neglected in interpreting the results and are essential for constructing the phase diagram for FeCO_3 .

Such large coolings during adiabatic magnetization should be possible only for Ising antiferromagnets whose intrasublattice exchange interaction J_{nnn} is either antiferromagnetic or else ferromagnetic but small. It is well known that in the molecular field approximation, T_f vanishes for ideal two-sublattice Ising antiferromagnets with $J_{nnn} = 0$ which are adiabatically magnetized in a field H_p equal to the

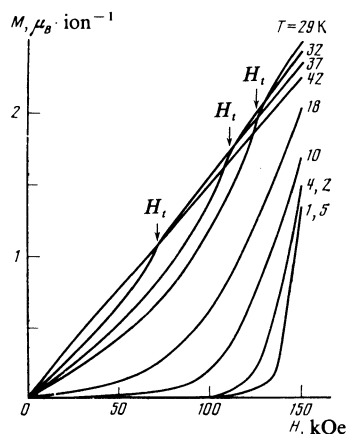


FIG. 2. Magnetization isotherms for siderite versus strength of dc magnetic field $H \parallel C_3$.

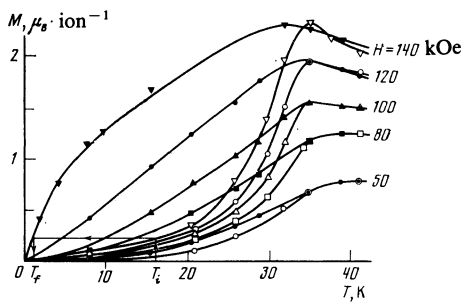


FIG. 3. Deducing the sample temperature during pulsed magnetization of siderite by comparing the curves $M(T)_H$ (experimental points \bullet , \blacksquare , \blacktriangle , \blacktriangledown) and $M(T_i)_H$ (\circ , \square , \triangle , \triangledown).

phase transition field, provided $T_i < 2/3 \cdot T_N$ (Ref. 30). The constant-entropy curves for such an AFM are dashed in Fig. 4a; the critical transition field H_i is taken to be the average $(H_1 + H_2)/2$. For H not too close to H_1 , the experimental points are closely approximated by the constant-entropy curves for the simple AFM model, which indicates that the exchange interaction among second neighbors is weak in FeCO_3 . On the other hand, the experimental points lie below the corresponding curves as H approaches H_1 . This indicates first that the phase transition actually occurs at $H = H_1$ and not at $(H_1 + H_2)/2$, and second that the transition must be accompanied by a sudden increase in the specific heat—this increase is responsible for the pronounced adiabatic cooling, which is stronger than expected for an AFM with $J_{nnn} = 0$ and $H_i = (H_1 + H_2)/2$. This situation is to be expected for antiferromagnetic intrasublattice exchange coupling; by contrast, a ferromagnetic coupling could suppress the spin fluctuations and diminish the cooling effect, as is observed in Ising antiferromagnets which exhibit metamagnetic behavior.³¹

4. MAGNETIC PHASE STATES AND PHASE TRANSITIONS

4.1. We are primarily interested in whether siderite crystals consist of a single magnetic phase in the field interval $H_1 < H < H_2$, or whether they contain both antiferromagnetic and paramagnetic domains. Because the difference in the Faraday rotation Φ in these domains may reach 1000

deg/mm for a metamagnetic AFM \rightarrow PM transition, one would expect that crystals of width less than 1 mm would depolarize linearly polarized incident light almost completely. In the first experiments, which were carried out for sample temperature $T = 25$ K, depolarization was in fact observed for light traveling across the siderite parallel to the C_3 axis in a magnetic field of strength between H_1 and H_2 . Circularly polarized light was not appreciably depolarized, from which we concluded that the polarization of the partially depolarized light can be pictured as a “fan” of polarization planes. Since magnetic rotation of the polarization plane is the only possible mechanism for light traveling along the optic axis of a centrosymmetric crystal, the depolarization must be attributed to a nonuniform distribution of the magnetization in the siderite. Experiments using crystals of various thicknesses revealed that the distribution is nonuniform in the bulk of the crystal, while experiments using a diffracted light beam of diameter down to $60 \mu\text{m}$ showed that the inhomogeneities are unrelated to spatial variations in the demagnetizing fields, and that their characteristic diameter is much less than $60 \mu\text{m}$. It might appear that only a magnetic phase stratification could account for this depolarization. However, estimates of the magnitude of the magnetic inhomogeneities required to explain the observed magnitude of the depolarization give values that are implausibly high. For crystals thin enough so that the depolarization $D = 1 - (I_{\text{max}} - I_{\text{min}})/(I_{\text{max}} + I_{\text{min}})$ was less than 0.5, the formula

$$\frac{(\overline{\delta M^2})^{1/2}}{\bar{M}} = \frac{1}{\Phi} \left(\frac{D}{2} \right)^{1/2}$$

relates D to the root-mean-square deviation $(\overline{\delta M^2})^{1/2}$ of the magnetization from the mean value \bar{M} for cylindrical regions of the crystal which are parallel to the vector \mathbf{k} and have transverse dimensions of at least $\lambda \times \lambda$. This formula implies that $(\overline{\delta M^2})^{1/2} \sim 0.04 M_{\text{sat}}$. On the other hand, the difference between the magnetic moments for the PM and AFM phases is comparable to M_{sat} . If we assume that the PM and AFM phases coexist in the crystal, then δM can be small only if the light is obliquely incident on the domain walls (this is because the interphase boundaries should ori-

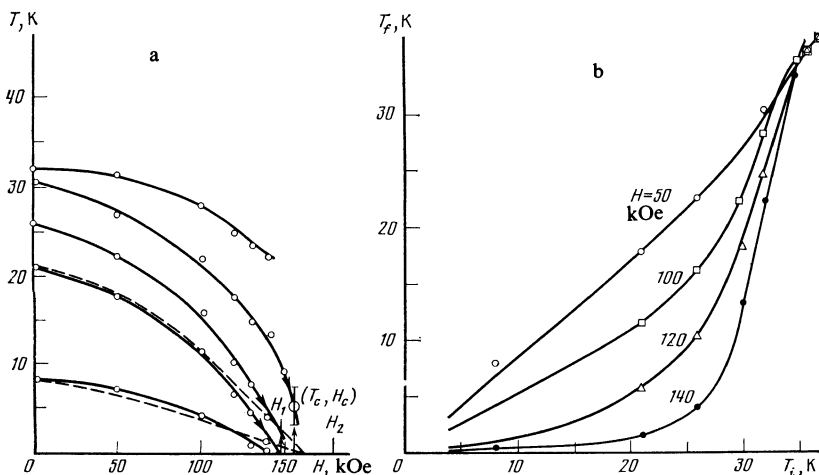


FIG. 4. Cooling of a siderite crystal with increasing pulse strength (a), and final temperature T_f as a function of the initial temperature T_i of the sample for several pulse amplitudes (b).

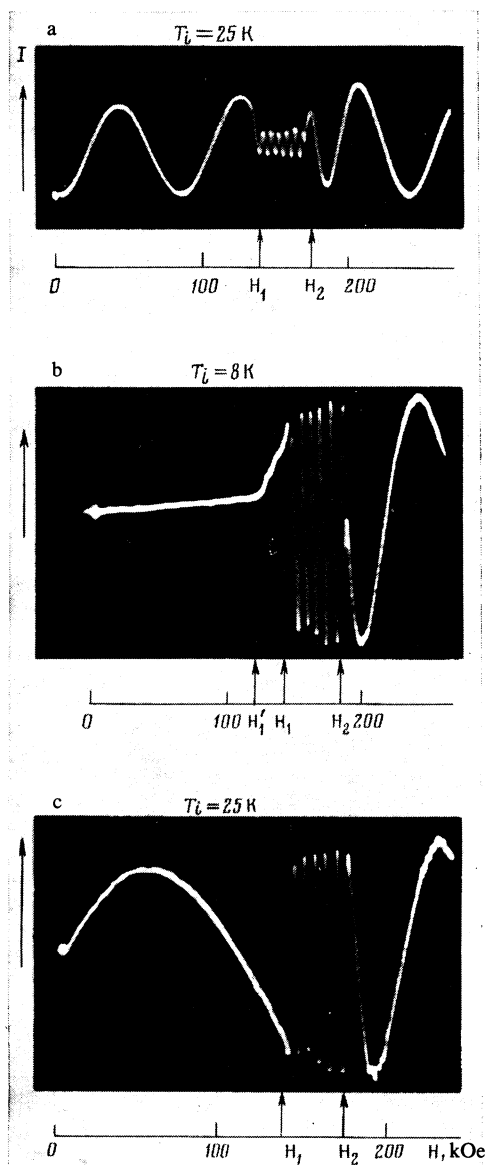


FIG. 5. Depolarization of siderite. The increase of the Faraday rotation angle to 10π is responsible for the oscillations in the light intensity $I(H)$ transmitted by the polarizer-sample-analyzer system. The decrease in the oscillation amplitude (a) indicates that the polarization of the light beam was spatially inhomogeneous; trace a was recorded before and traces b, c after cryomagnetic treatment, in which a field pulse of amplitude 250 kOe was applied; $T_i = 8$ and 25 K for b and c, respectively. Sample thicknesses: a) 1.45 mm; b, c) 1.05 mm; $\lambda = 6328 \text{ \AA}$.

ent themselves parallel to the magnetic field, particularly when the magnetic moments in the two phases differ widely). The angle of incident θ must be greater than d/t , where d is the period of the domain structure and t is the thickness of the crystal. If the divergence of the laser beam is small, we would expect D to increase when θ varies so that the angle between \mathbf{k} and the plane of the domain walls decreases. However, we did not observe any appreciable change in D when θ changed several degrees. In addition, for angles $2\Omega \lesssim 20^\circ$ we did not detect any diffraction associated with the possible formation of a small-period magnetic domain structure. These negative findings make phase stratification seem im-

plausible. Moreover, if we nevertheless assume that a domain structure formed, then the structure would be only metastable for fields $H_2 - H_1 > 4\pi\Delta M$ and one would not expect the domain dimensions to change gradually [the latter is required in order to account for the smallness of the depolarization and for the smooth behavior of $I(H)$]. We think it more likely that the depolarization is due to weak magnetic inhomogeneities associated with structural defects in the crystal which are generated at threshold fields. Because of the magnetoelastic coupling, the resulting elastic stresses induce local changes in the magnetization. Estimates show that elastic stresses of order 10^3 kg/cm^2 can provide the required change of $\approx 10^{-2} M_{\text{sat}}$.

The experiments with samples cooled below 8 K provided unexpectedly strong evidence for the lack of a two-phase AFM \rightarrow PM structure for $H_1 < H < H_2$. No depolarization was noted in these samples, nor was it observed after the samples were warmed to 25 K, or to 290 K followed by re-cooling to 25 K (Fig. 5). Moreover, depolarization was not found even in freshly prepared crystals at $T = 25 \text{ K}$ during the first few field pulses—several strong field pulses were required to produce depolarization. The properties and the small magnitude of the depolarization of light in freshly prepared specimens support the hypothesis that the depolarization was associated with structural defects generated at threshold field strengths. These defects are reversible initially, but the subsequent field pulses make them permanent. The irreversible disappearance of the depolarization properties of siderite at lower temperatures could be due to an enhancement of the effects of dynamic magnetostriction acting on the crystal defects, with the result that local elastic stresses may be eliminated irreversibly through the formation of microcracks, extrusion of dislocation pile-ups to the surface of pores, etc.

The smooth change in the Faraday rotation Φ and the behavior of D in siderite for fields $H_1 < H < H_2$ thus lead us to conclude that pulsed magnetization of the antiferromagnetic FeCO_3 results in a state which is neither AFM nor PM; although the characteristic dimension of the new structure may be incommensurate with the period of the elementary cell, it is in any case less than the wavelength of the light. The properties discussed above suggest that a single-phase magnetic state may be involved. We will henceforth refer to it somewhat arbitrarily as a mixed or C-state (as was suggested in Ref. 20), where just as for the case of type-II superconductors the word "mixed" does not indicate the physical coexistence of separate phases but rather a mixture of phase properties. In other words, in the mixed state the geometric dimensions of the regions comprising the two phases are comparable to the lattice constant. The C-state in FeCO_3 can also be regarded as an AFM state in which the density of soliton excitations is such that their interactions give rise to a dynamic or stationary cooperative state.

4.2. In addition to the depolarization of light, which was observed in a wide field interval $H_1 < H < H_2$ for specimens not subjected to cryomagnetic treatment, we also found peaks in the intensity $I(H)$ of the light transmitted by the polarizer-sample-analyzer system; the peaks were confined to narrow intervals $H \approx H_1$ and $H \approx H_2$. The changes in

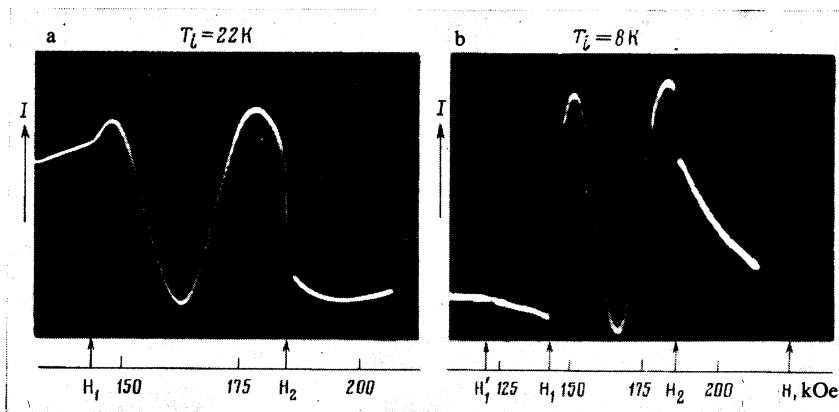


FIG. 6. Behavior of $I(H)$ near H_1 and H_2 for a specimen of thickness 0.45 mm.

$I(H)$ for $H \approx H_2$ were most abrupt for crystals that were not exposed to strong magnetic fields at low temperatures. For specimens of thickness 1.45 mm and initial temperature $T_i = 25$ K, the amplitude of the oscillation near H_2 was almost 10 times smaller. The peaks became sharper after cryomagnetic treatment at $T = 8$ K. By moving the polarizer and changing the sample thicknesses, we were able to observe several different features in the (H) curves—a spurious low-amplitude oscillation, a narrow horizontal shelf, and an abrupt jump (the number of true oscillations was deduced from the dependence $I(H)$ on the trailing edge of the field pulse, where the oscillating dependence was devoid of unusual features). We can understand this behavior by assuming that a first-order magnetic phase transition occurs at H_2 , and the crystal breaks up into domains of two phases whose boundaries are parallel to the magnetic field and which have different Faraday rotations. The abrupt jump in $I(H)$ in the oscilloscope traces for thin specimens (Fig. 6) and the discontinuities in $\Phi(H)$ (Fig. 7) deduced from the traces indicate unambiguously that the magnetic moment of the crystal changes abruptly at $H = H_2$. Only a first-order phase transition could account for this change. The magnitude ΔM of the jump can be calculated from the jump in the Faraday rotation, which was equal to 110 deg/mm for $T_i = 22$ K and 73 deg/mm for $T_i = 6$ K. The corresponding jumps ΔM are equal to 71 and 47 emu/cm³. The drop in ΔM with decreasing temperature could be due to an increase in the nucleation time for the new PM phase, since the magnetization of the old C-phase increases with H faster than M for the PM phase.

The behavior of $I(H)$ near H_1 is different. The decrease in the oscillation amplitude occurs in a larger field interval of width ~ 5 kOe (as compared with ~ 1 kOe near H_2); moreover, the magnitude of the decrease is much smaller (at most 10%), and it is difficult to detect (see Fig. 5) and differs for different samples. Although a kink near H_1 can be discerned in the traces recorded for thin crystals with $T = 22$ K, no jump is present. When T_i decreases to 6 K, the slope of $I(H)$ increases near H_1 , but $\Phi(H)$ remains smooth (see Fig. 7). If as in Fig. 7 we take H_1 for $T_i = 6$ K to be the field at which $\Phi(H)$ has a kink, $\Phi(H)$ varies exponentially for $H \lesssim H_1$ (see the insert to Fig. 7). The continuous behavior of $\Phi(H)$ indicates that even at $T_i = 6$ K the phase transition at $H = H_1$ is second-order (for an initial temperature $T_i = 6$ K, the anticipated crystal temperature is less than 0.5 K at $H = H_1$, see Fig. 4).

The curve $\Phi(H)$ can be used to estimate the maximum differential magnetic susceptibility for $H > H_1$; we get the value 0.08–0.09 emu/cm³, which is only slightly less than $1/N_z = 0.12$ emu/cm³, the maximum possible susceptibility of the crystal (here $N_z \approx 8$ is the demagnetizing factor for siderite). We expect that at lower temperatures, the demagnetizing fields will cause the second-order transition at $H = H_1$ to become first-order for crystal wafers cut perpendicular to the C_3 axis.

Although the existence of the phase transitions at $H = H_1$ and H_2 is beyond dispute, measurements in pulsed fields alone cannot establish whether the transitions in FeCO₃ are equilibrium or kinetic processes. To answer this question we measured M and χ in strong dc fields.

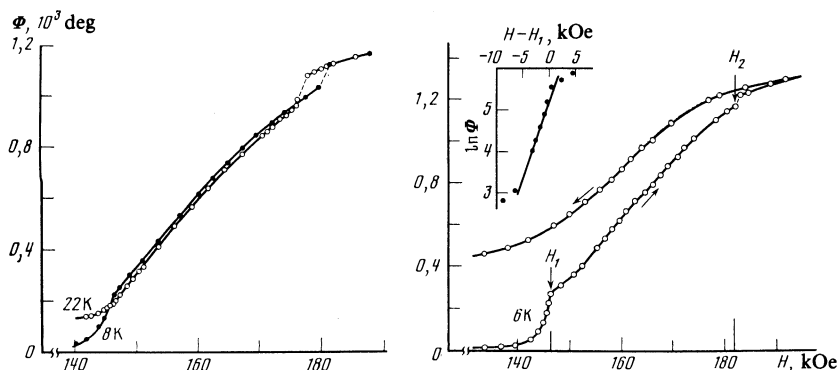


FIG. 7. Faraday rotation in siderite during the AFM→C-state→PM magnetic transition in a pulsed field.

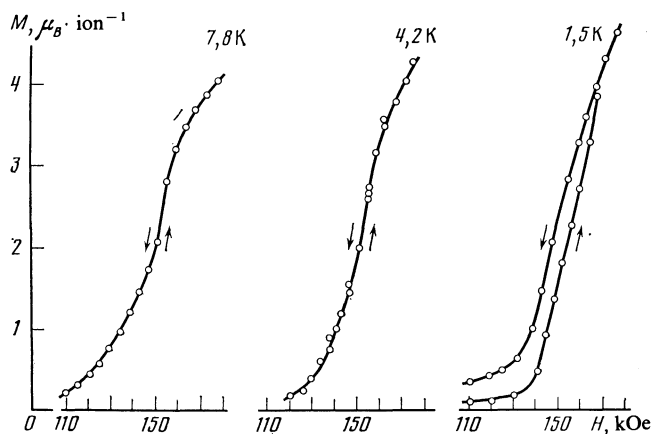


FIG. 8. Magnetization of siderite during the magnetic transition in a dc field.

The qualitative form of $M(H)$ for siderite in dc fields changes as T decreases. Thus, although $M(H)$ has distinct kinks corresponding to AFM→PM phase transitions (Fig. 2) at high temperatures, for $T < 8$ K, M peaks abruptly inside the transition interval of width 30–40 kOe (Fig. 8). The fine structure of the magnetic transition can be determined only by measuring the differential magnetic susceptibility (Fig. 9). The peak in $\chi(H)_T$ at first becomes sharper as T drops below 7 K, but broadening followed by a splitting of the peak occurs for $T < 4.2$ K. Figure 9 clearly shows two peaks in the plateau-shaped curve $\chi(H)_T$ for $T = 2$ and 1.5 K.

The behavior of the isothermal curves $\chi(H)_T$ is consistent with the results from the pulsed measurements if we allow for the adiabatic cooling of the crystal during the pulsed magnetization. The characteristic features of the $\Phi(H)$ curves for pulsed fields and $T_i = 6$ K are much more pronounced than for the $M(H)_T$ curves recorded in a steady field at $T = 1.5$ K. The most likely explanation is that in the pulsed measurements the magnetic transition occurred at lower temperatures than the lowest temperature 1.5 K for which the isotherms were recorded. Although one cannot completely rule out the possibility that the phase transition may have been kinetic (nonequilibrium), particularly at the field H_1 , the threshold fields H_1, H_2 were nevertheless nearly identical for the pulsed and the dc measurements. This indicates that at least qualitatively, the AFM→C-state→PM magnetic transition proceeded in thermodynamic equilibrium in the pulsed measurements.

4.3. The $\Phi(H)$ curves for siderite in pulsed fields have an additional feature that was not discussed above—the traces $I(H)$ show a distinct kink at $H'_1 = 123$ kOe (see Figs. 5 and 10) for $T_i = 8$ K in crystals of good optical quality, and the kink is still discernible for $T_i = 17$ K ($T_f = 1$ K). For increasing $H > H'_1$, $\Phi(H)$ rises almost linearly with H ; thereafter, the growth becomes exponential as H approaches H_1 . It is difficult at this point to say anything specific regarding the physical nature of this behavior; however, the fact that a kink is observed only for high-quality crystals suggests that it is not associated with impurities but rather reflects the properties of the Fe^{2+} magnetic subsystem. The kink could

be due to formation of the C-phase, which is stabilized by exchange interactions among remote Fe^{2+} ions (third coordination sphere and beyond). The kinks are not present in the $M(H)$ curves recorded for dc fields, presumably because the measurements were not carried out at sufficiently low temperatures.

5. HYSTERESIS PROPERTIES OF SIDERITE

Figures 1 and 7–11 illustrate the fundamental hysteresis properties of the Faraday rotation for various pulsed field amplitudes and initial sample temperatures. The hysteresis becomes appreciable once H reaches H'_1 and thereafter increases with H . If $H > H'_1$ is sufficiently close to H'_1 the features of $I(H)$ at H_1 and H'_1 are reproduced on the trailing edge of the field pulse (traces *a* and *b* in Fig. 10). As H approaches H_2 , the features become broader and less distinct. Nevertheless, $I(H)$ has characteristic kinks for $H \approx H_1$ and H'_1 (Fig. 10c), indicating a departure from smooth oscillations. As soon as H becomes greater than H_2 , the kinks at H'_1 and H_1 are no longer reproduced on the trailing edge of the pulse. The field interval $H < H_1$ contributes substantially to the area S of the hysteresis loop (see Fig. 1). Figure 11a plots $S(H)$ in energy units. We see that S jumps abruptly at $H = H_2$, more than doubling in value. S decreases as T rises and vanishes at $T_i \approx 31$ K. The $\Phi(H)$ curves recorded in the backward direction (decreasing H) for several T_i are all similar (but not identical to) the zero-hysteresis curve recorded for $T_i = 31$ K (see Fig. 1). A small hysteresis may be noted for quasistatic fields and temperatures below 4.2 K (Fig. 8); its area is equal to 0.5 J/cm^3 , as compared with $S = 3 \text{ J/cm}^3$ for the pulsed experiments.

The nature of the magnetic hysteresis in siderite has been discussed in Refs. 16, 21, 25, and 26. It was suggested¹⁶ that the magnetic transition in siderite is an ordinary first-order metamagnetic phase transition which is washed out by spatial variations in the exchange fields that act on the magnetic ions in crystals with high impurity concentrations, while the hysteresis is due to the action of the field pulse, which retards the transition. The intensity and shape of the electron absorption bands in siderite were analyzed spectro-

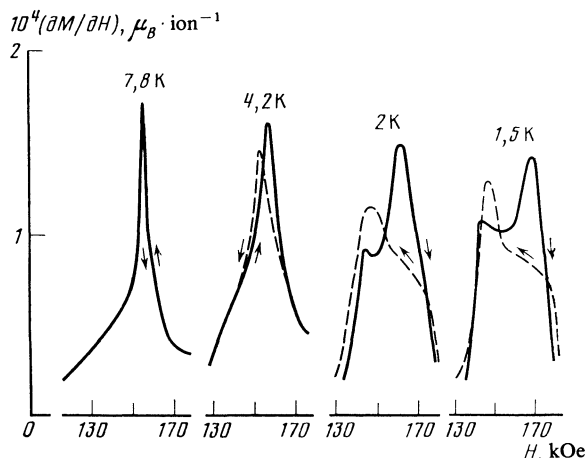


FIG. 9. Differential magnetic susceptibility of siderite recorded for dc fields close to the transition field H_1 .

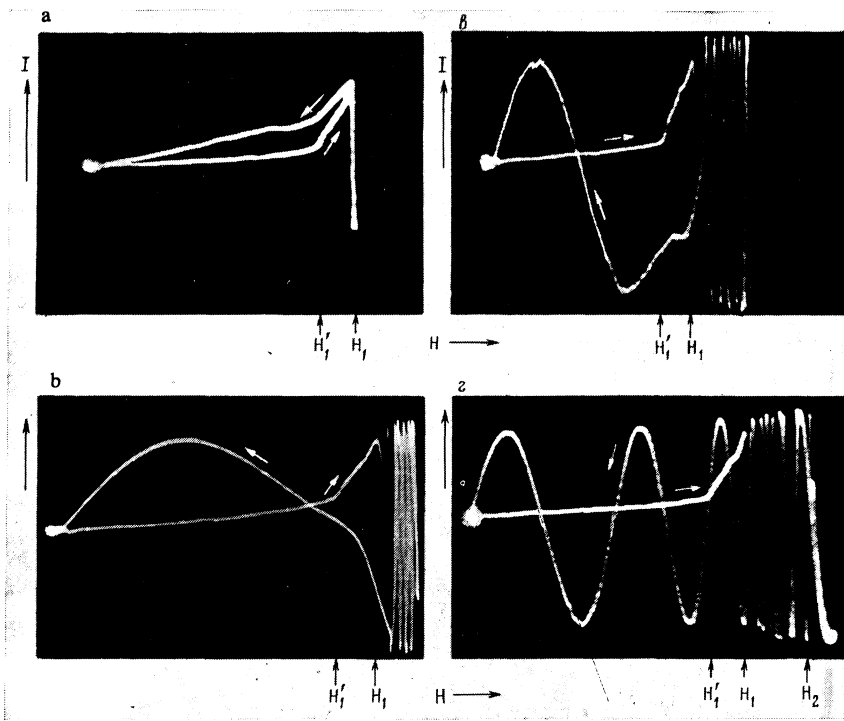


FIG. 10. Hysteresis in $I(H)$ for four different pulse amplitudes: a) $H_a \approx H_1$; b) $H_a > H_1$; c) $H_a \lesssim H_2$; d) $H_a > H_2$.

scopically in Ref. 25, where it was concluded that the sample temperature increases abruptly to 24 K once H reaches H_1 and thereafter rises to 27–28 K; however, the temperature was ≈ 24 K at the instant the field pulse terminated. The difference between the $M(H)$ curves for the leading and trailing edges of the pulse was ascribed to irreversible heating when H reached the threshold value H_2 . In Ref. 26 an attempt was made to explain this heating for a metamagnetic siderite model (i.e., $J_{nn} < 0$ and $J_{nnn} > 0$); irreversible absorption of energy from the time-varying magnetic pulse near the critical point was assumed to be the dominant process, and the liberation of the latent heat of transition was taken to be responsible for heating the sample to the critical temperature. On the other hand, an AFM siderite model with exchange interactions among ions in the same sublattice (i.e., $J_{nn}, J_{nnn} < 0$) was considered in Ref. 21, and the hysteresis was attributed not to heating but to the long time required for equilibrium multisublattice C-phase structures to form, and to the existence of a metastable nonequilibrium C-state down to zero fields.

We attempted to determine the change in the sample temperature from measurements of $M(H)$ and $\Phi(H)$ in dc and pulsed fields. The change in temperature for increasing

$H < H_1$ was found above and is shown in Fig. 4. The sample temperature in a decreasing field $H > H_1$ was found from the intersection point of the curves $M(H_{dc}, T = \text{const})$ and $M(H_{\text{pulse}}, T_i)$ by assuming equilibrium $M(H)$ dependences for both the dc (quasistatic) and pulsed fields. Figure 12a plots $M(H)$ for dc fields at various temperatures, along with $K^{-1}\Phi(H_{\text{pulse}})$ for the leading and trailing edges of the pulse for $T = 8$ K and two pulsed field amplitudes $H_a < H_2$ and $H_a > H_2$.

We estimated the sample temperature for $H < H_2$ by comparing the curve $M(H_{\text{pulse}}, T_i = 8 \text{ K})$ with isotherms $M(H)_T$

$$M = M_0 \tanh x, \quad x = \frac{\mu H_t}{kT} \left[\frac{H}{H_t} - (1 + \gamma) \frac{M}{M_0} \right] \quad (1)$$

calculated in the molecular field approximation for the paramagnetic state of an Ising antiferromagnet. Figure 12b shows the results, which were calculated for $\mu = \mu_{\text{Fe}^{2+}} = 5 \mu_B$ and

$$\gamma = J_{nnn}/J_{nn} = (H_2 - H_1)/(H_2 + H_1) = 0.1, \quad H_t = 1/2(H_1 + H_2).$$

The points where the experimental curve A intersects the isotherms give the field H at which the corresponding tem-

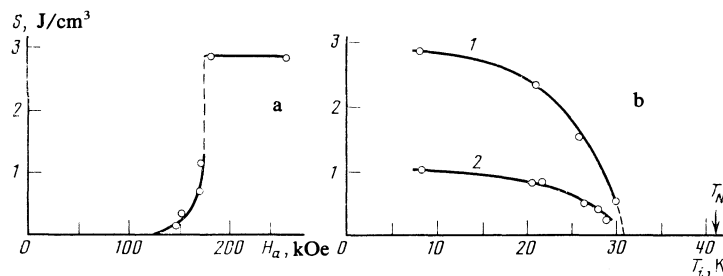


FIG. 11. Hysteresis properties of siderite: area of hysteresis loop vs pulse amplitude (a) and as a function of initial sample temperature (b); 1) $H_a > H_2$; 2) $H_2 > H_a > H_1$.

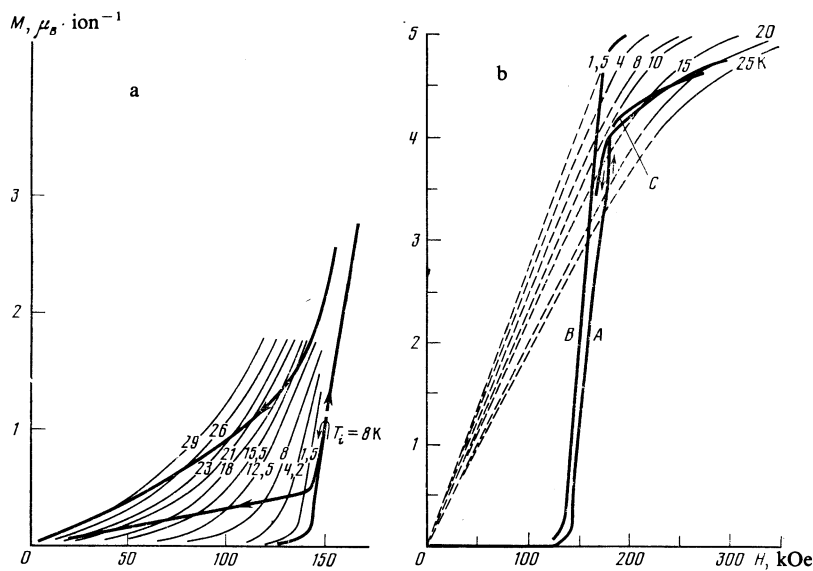


FIG. 12. Diagrams showing how the sample temperature is determined for fields $H < H_1$ on the trailing edge of the pulse (a) and for $H > H_2$ on both edges (b). a) The light curves show the experimental isotherms $M(H)_T$, while the heavy curves plot $M(H)_T$ -deduced from the Faraday rotation for pulsed fields. b) The light curves are show isotherms $M(H)_T$ calculated for $H > H_2$; curves A, B, and C show the experimental dependences $M(H)$; A was deduced from the Faraday rotation; C is taken from Ref. 18; the isotherm B was recorded at $T = 1.5$ K for $H < 180$ kOe.

perature was reached. Figure 12b also presents an experimental isotherm $M(H, T = 1.5$ K) recorded for $H < 180$ kOe (curve B), which shows the degree to which the Fe^{2+} magnetic moment assumed in the calculations is satisfactory. Curve C plots the dependence¹⁸ $M(H_{\text{pulse}}, T = 4.2$ K) and gives an indication of the agreement in the results of different experiments using different samples.

Figure 13 plots the sample temperature $T(H)$ as a function of the field strength. The striking similarity between the constant-entropy curve for $T_i = 30$ K and the $T(H)$ curve for decreasing $H < H_1$ and $H_a > H_2$ indicates that the siderite was in magnetic equilibrium on the back (falling) edge of the pulse. The final temperature at the instant the field pulse terminated was $T_f = 29$ K. In addition, the shape and width of the optical absorption bands give $T_f \approx 26$ K (Refs. 25, 26). On the other hand, for $H > H_2$ our temperatures T_f do not agree so well with the results found in Refs. 25 and 26. Our data for $H \gtrsim H_2$ give $T_f \approx 12$ K, as against 27–28 K there. In order to explain this large discrepancy, we must assume that local heating of the magnetic subsystem can occur and take the spin-lattice relaxation time in the bulk of the crystal to be greater than 10^{-3} s. These assumptions hardly seem reasonable for such low temperatures. The discrepancy could conceivably be due to ambiguities in interpreting changes in the shape of the complicated siderite absorption bands in the magnetic field. Difficulties in interpreting the optical spectrum may also account for the different field dependences $T_f(H)$ found in Refs. 25 and 26.

The above discussion leaves no doubt that irreversible heating, which occurs primarily during the transition from the mixed C to the paramagnetic PM states at $H = H_2$, qualitatively alters the behavior of the magnetization of siderite in a decreasing pulsed field. The most plausible explanation is that the heating results from the nonequilibrium nature of the C-state in an increasing field. Neither the second-order phase transition at $H = H_1$ nor the dependence $H_2(T)$ is consistent with the conjecture in Ref. 26, according to which the evolved latent heat of transition heats the sample up to the critical temperature. Moreover, the estimates given there

for the amount of energy that the crystal absorbs from a slowly time-varying pulsed field near the critical point are also too optimistic. On the other hand, it was conjectured in Ref. 21 that the PM \rightarrow C-state transition time is long and that the formation of the metastable C-state is delayed even down to zero fields; however, this explanation is inconsistent with the essentially equilibrium dependence $M(H)$ in decreasing fields and with the high final temperatures T_f . Because of possible large errors in measuring the absolute field strengths when recording $M(H)$ in the various experiments, we have no quantitative data on the degree of nonequilibrium of the magnetization process. Nevertheless, the available data suggest that some deviation from equilibrium occurred. Although the interval $H_2 - H_1 = 35$ kOe found from the pulsed experiments is similar to the interval obtained by extrapolating H_1 and H_2 deduced from dc measurements to 0.5 K, the actual critical fields H_1, H_2 for static fields are weaker. The potential magnetic energy stored up in the non-equilibrium C-state should be converted into heat most effectively during formation of the PM state. An irreversible jump-like increase in the temperature may be expected to occur in fields $H \gtrsim H_{2\text{eq}}$ if the walls separating domains in the PM and metastable C-state move, or if the C-state is destabilized and rapidly transformed into the paramagnetic

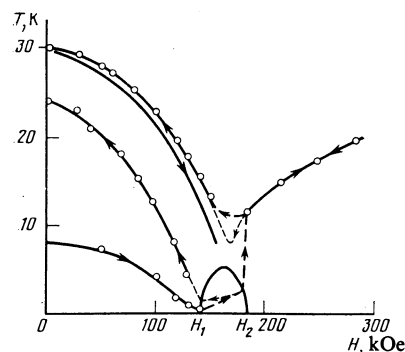


FIG. 13. Cooling of the sample during a magnetic field pulse. The dashed parts of the curves correspond to nonequilibrium states.

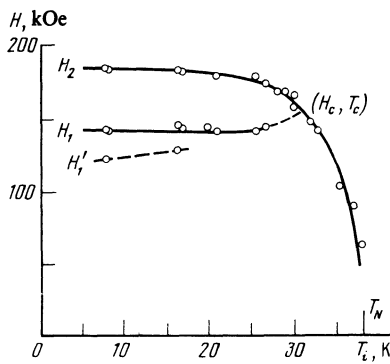


FIG. 14. The fields H_1' , H_1 , and H_2 as functions of the initial sample temperature T_i (from pulsed-field measurements).

state.

For quasistatic fields the magnetization process lasts for several minutes, and the hysteresis in this case is of interest even though it is not pronounced under these conditions (see Fig. 8). For low temperatures ($T = 4.2$ K), a small hysteresis appears in $\chi(H)$ for fields $> H_1$, and at $T = 1.5$ K the area of the hysteresis loop is equal to 0.5 J/cm^3 . We attribute this hysteresis to various processes involving the magnetic viscosity. Irregular local variations in the exchange parameters due to crystal imperfections and impurities in naturally occurring siderite may also play a role. Microscopic changes of composition in the presence of a field may give rise to ferromagnetic centers whose relaxation time becomes quite long after the field is decreased.

6. MAGNETIC PHASE DIAGRAM

The $T(H)$ curves in Fig. 4 for the cooling on the leading edge of the pulse can be used to find the H, T phase diagram for FeCO_3 by using the $\Phi(H)$ dependence recorded for pulsed fields and various initial sample temperatures T_i . Figure 14 shows the state diagram in the H, T_i plane. The fields H_1 and H_2 were found from the position of the kinks and jumps; on the $I(H)$ traces and from $\Phi(H)$ (Figs. 1, 5–7). For the higher temperatures, the phase transition field H_1 was identified with the field for which the slope $d\Phi(H)/dH$ was a maximum. In constructing the diagram in the H, T_i plane, we found the temperature coordinates of points on the curve $H_1(T_i)$ from the intersections of the vertical lines $H_1(T_i) = \text{const}$ with the curve $T_f(H)_{T_i}$ (cf. Fig. 4a). The only thing we can say regarding the crystal temperature at the times when $H = H_2$ is that it was less than T^* (less than $0.8 T^*$ for $T_i < 25$ K); here T^* is the temperature below which the C-state can form and the transition to the PM state occurs via two phase transitions. This conclusion follows from the fact that the behavior of $\Phi(H)$ for $H \approx H_2$ ($H < H_2$) is quite different from the $\Phi(H)$ dependence at $T_i = 30$ K, and from the fact that for crystals not subjected to strong fields at low temperatures the depolarization D of the light decreased only slightly as H increased to H_2 . Indeed, D remained greater than the value observed for H slightly larger than H_1 at $T_i = 27$ K. On the other hand, the temperature $T_i = 27$ K corresponds to $T_f(H_1) \approx (3-4) \text{ K} = (0.4-0.8) T^*$, where $T^* = 6 \pm 2$ K. We used the follow-

ing method to determine the coordinates T^* and H^* of the point (H^*, T^*) which is farthest from the H axis and lies on the curve demarcating the upper temperature bound for existence of the C-state. We found $H^* = 155$ kOe and $T_i^* = 31$ K from the dependences $H_1(T_i), H_2(T_i)$ by extrapolating $H_1(T_i)$ up to the intersection point with $H_2(T_i)$ (see Fig. 14). We then found $T^* = 6$ K by extrapolating the corresponding curve $T_f(H, T_i = 31 \text{ K})$ to $H = H^* = 155$ kOe (Fig. 4a). The error in T^* was estimated at ± 2 K. One can also determine T^* from the temperature at which the hysteresis vanishes. Indeed, the $S(T_i)$ curve (see Fig. 11b) shows that the area of the hysteresis loop vanishes as T_i approaches the same value 31 K as above. Moreover, the jump in the Faraday rotation at $H = H_2$ can still be made out for temperatures as high as 27 K, which is close to the value $T_i = 31$ K. This near-equality suggests that T^* should be close to (if not equal to) T_c , the temperature at which the first-order phase transition vanishes in the magnetic field. In any event, given the error in determining T^* we may assume that $T_c = T^*$. We note that in essence, the point (T_c, H_c) is a triple critical Lifshitz point,^{33,34} and the C-state is a modulated phase.

In constructing the phase diagram curves from the magnetic measurements in quasistatic fields, we deduced the transition fields H_i from the positions of the kinks in $M(H)$ and the peaks in the susceptibility $\chi(T)$ (see Figs. 2 and 9). The critical temperature was close to 4 K—this follows from the fact that two peaks are distinctly visible for $T = 2$ K while only one narrow peak is observed at 7.8 K, and at $T = 4.2$ K the peak is appreciably broadened and a small hysteresis appears in $\chi(T)$. According to Fig. 9, the critical field H_c is close to 154 kOe. Figure 15 shows some curves on the magnetic phase diagram for FeCO_3 . The general form of the diagram is clear even though the experimental points for pulsed and quasistatic fields do not agree completely.

It will be of interest to compare this state diagram with the one for a cubic antiferromagnet with AFM exchange interactions between nearest and second-nearest neighbors; such a diagram was constructed in Ref. 23 in the mean-field approximation. The similarity with the diagram for FeCO_3 is striking—in both cases there is a region of third phase (neither AFM nor PM) which is bounded from below by a line of second-order phase transitions and from above by a line of first-order transitions; the critical point is the one farthest from the H axis on the curve giving the upper temperature bound for the existence of the third phase. The distinctive feature of the diagram in Ref. 23 is that the region in which the third phase exists is bounded by the AFM region everywhere except at the point $T = 0$ K, and for $T < T_c$ and AFM \rightarrow PM second-order phase transition also occurs. However, the latter transition is not pronounced and occurs for fields $H \approx H_i$, where H_i is the critical field for the C-state \rightarrow AFM transition (the two fields become equal as $T \rightarrow 0$ K).

According to Ref. 23, the critical temperature T_c is given by the ratio

$$T_c = \frac{J_{nnnz_{nnn}}}{J_{nnz_{nn}} T_N}, \quad (2)$$

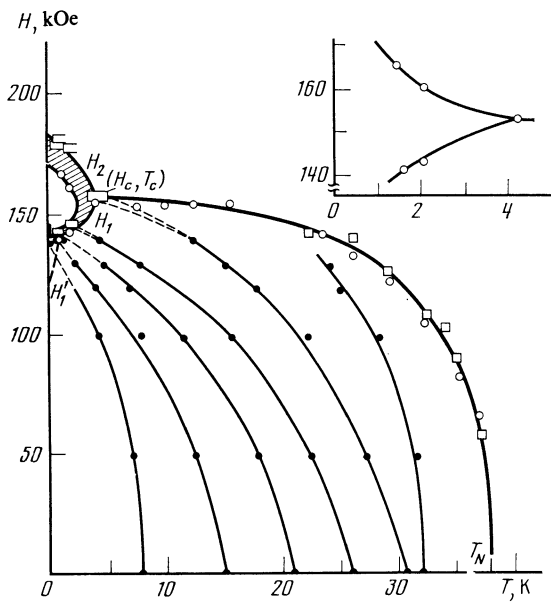


FIG. 15. Magnetic phase diagram for FeCO_3 deduced from pulsed (\square) and dc (\circ) magnetic field experiments. The light lines are curves of constant entropy. The insert shows the expected behavior of the curves in the diagram near the critical point T_c . The hatched region shows the error in determining the positions of the curves.

where z_{nn} and z_{nnn} are the numbers of nearest and next-nearest neighbors, and the couplings J_{nn} , J_{nnn} correspond to the Hamiltonian

$$\mathcal{H} = - \sum_i (J_{nn} z_{nn} \langle S_i S_{nn} \rangle + J_{nnn} z_{nnn} \langle S_i S_{nnn} \rangle). \quad (3)$$

Using (2) to estimate J_{nnn}/J_{nn} for siderite, we find that $J_{nnn}/J_{nn} = 0.11$ for $T_c = 4$ K if we set $z_{nnn} = z_{nn}$. This result is very close to the value

$$J_{nnn}/J_{nn} = (H_{2in} - H_{1in}) / (H_{1in} + H_{2in}) \quad (4)$$

given by the two-sublattice model. Here H_{1in} and H_{2in} are the threshold internal fields; using the pulsed measurements to allow for the effect of the demagnetizing field, we can take $H_{1in} \approx H_1 = 147$ kOe and $H_{2in} = H_2 - 6$ kOe = 177 kOe. By comparison, we find $H_{1in} = 135$ kOe and $H_{2in} = 170$ kOe if we linearly extrapolate H_1 and H_2 to 0, with H_1 and H_2 measured experimentally for dc fields. We then find $J_{nnn}/J_{nn} = 0.09$ and 0.11, respectively. The exchange parameters are then given by

$$J_{nn} z_{nn} = -\mu (H_1 + H_2) / 2S_z^2, \quad J_{nnn} z_{nnn} = -\mu (H_2 - H_1) / 2S_z^2. \quad (5)$$

If we substitute the values for H_{1in} , H_{2in} and $S_z = 2$, $\mu = 5\mu_B$, we find that $J_{nn} z_{nn} / k = -12.8 \pm 0.5$ K and $J_{nnn} z_{nnn} / k = -1.3 \pm 0.1$ K.

When T drops below T_c/z_{nnn} , new phase transition curves should appear in the state diagram due to the formation of magnetic superstructures whose period changes abruptly. Spikes on the differential susceptibility curve were observed in Ref. 20, where they were attributed to such superstructures. We believe that the absence of spikes in the quasistatic experiments at $T = 1.5$ K was due to the fact that the temperature 1.5 K was not low enough. On the other

hand, the cooling in the pulsed experiments with $T_i = 4.2$ K produced sufficiently low temperatures, and the susceptibility spikes may be attributed to equilibrium or metastable transitions between different commensurate structures. The decreased spike amplitude for faster-rising field pulses noted in Ref. 20 might indicate that the magnetic system approached equilibrium,²⁰ or it could reflect heating of the spin subsystem due to spin-lattice relaxation at a higher lattice temperature. If we write $(Jz)_n$ for the interaction between remote neighbors lying beyond the second coordination sphere, then when T drops further to $\sim T_c (Jz)_n / (Jz)_{nnn}$ new transition curves may appear in the diagram if the antiferromagnetic interactions (for neighbors in the same plane) or ferromagnetic interactions (for neighbors in different planes) are sufficiently strong. Similar situations have been analyzed theoretically for several magnetic materials with competing interactions.³⁵ The observed behavior of the Faraday rotation for $H = H'_1$ could be a consequence of transitions of this type.

7. CONCLUSIONS

Our experiments imply that the antiferromagnet FeCO_3 differs qualitatively from ordinary classical two-sublattice metamagnets such as FeCl_2 , which have a strong ferromagnetic coupling between ions in the same sublattice together with a weaker AFM coupling, which induces an antiferromagnetic ordering. The classical metamagnets undergo a sharp AFM \rightarrow PM (FM) transition in magnetic fields. By contrast, FeCO_3 is a representative of the class of Ising antiferromagnets which have negative (AFM) exchange interactions between pairs of nearest-neighbor ions (in different sublattices) and between pairs of second-nearest neighbors (in the same sublattice); very little experimental or theoretical work has been done on such materials. The antiferromagnets in this class are of interest because the AFM \rightarrow PM transition in the presence of a magnetic field should give rise to new magnetic structures for sufficiently low temperatures; the period of these structures may be commensurate or incommensurate with the period of the ionic cell of the crystal. The structure should change in an applied field, or as the temperature is changed. The exchange interaction between remote neighbors and the presence of other weak interactions should be decisive in determining the period of the structures and their stability to thermal and quantum fluctuations. Studies of FeCO_3 may be useful in analyzing modulated magnetic structures and in verifying the predictions of the soliton theory, according to which the structural changes in commensurate soliton lattices are associated with the formation of incommensurate or metastable chaotic lattices. Experiments at $T < 1$ K using FeCO_3 single crystals grown in the laboratory should yield the most informative results.

¹Laboratoire L. Néel, Centre National de la Recherche Scientifique, Grenoble.

²Laboratoire de Magnétisme et Optique du Solide, Centre National de Recherche Scientifique, Meudon-Bellevue, France.

¹R. A. Alikhanov, Zh. Eksp. Teor. Fiz. 36, 1690 (1959) [Sov. Phys. JETP 9, 1204 (1959)].

- ²Y. Kanamori, *Prog. Theor. Phys.* **20**, 890 (1958).
- ³G. A. Prinz, D. W. Forester, and J. L. Lewis, *Phys. Rev.* **8B**, 2155 (1973).
- ⁴V. V. Eremenko, A. I. Maslennikov, and V. M. Naumenko, *Phys. Status Solidi (b)* **81**, 351 (1977).
- ⁵Yu. A. Popkov, V. V. Eremenko, V. I. Fomin, and A. P. Mokhir, *Fiz. Tverd. Tela (Leningrad)* **14**, 2294 (1972) [*Sov. Phys. Solid State* **14**, 1985 (1972)].
- ⁶P. B. Langille and D. C. O'shea, *J. Phys. Chem. Solids* **38**, 1161 (1977).
- ⁷D. E. Wrege, S. Spooner, and H. A. Grezsch, *AIP Conf. Proc.* **5**, 1334 (1973).
- ⁸J. W. Lynn, N. A. Mook, and W. J. Buyers, *Phys. Rev.* **B12**, 238 (1975).
- ⁹R. F. Altman, S. Spooner, and D. P. Landau, *AIP Conf. Proc.* **10**, 1163 (1978).
- ¹⁰D. W. Forester and N. C. Koon, *J. Appl. Phys.* **40**, 1316 (1969).
- ¹¹N. H. Ok, *Phys. Rev.* **185**, 472 (1969).
- ¹²A. Okiji and J. Kanamori, *J. Phys. Soc. Jpn.* **19**, 908 (1964).
- ¹³H. J. Bizette, *J. Phys. Radium* **12**, 161 (1951).
- ¹⁴M. Focx, *Ann. Phys.* **16**, 174 (1921).
- ¹⁵J. S. Jacobs, *J. Appl. Phys.* **34**, 1106 (1963).
- ¹⁶V. I. Ozhogin, *Zh. Eksp. Teor. Fiz.* **45**, 1687 (1963) [*Sov. Phys. JETP* **18**, 1156 (1963)].
- ¹⁷H. Cofta, *Metamagnetiki*, Warsaw (1971), p. 222.
- ¹⁸E. Stryjewski and N. Giordano, *Rev. Adv. Phys.* **26**, 487 (1977).
- ¹⁹V. V. Eremenko, K. L. Dudko, Yu. G. Litvinenko, V. M. Naumenko, and N. F. Kharchenko, in: *Int. Conf. Low Temp. Phys., Boulder (1972)*, p. 365.
- ²⁰K. L. Dudko, V. V. Eremenko, and V. M. Fridman, *Zh. Eksp. Teor. Fiz.* **68**, 659 (1975) [*Sov. Phys. JETP* **41**, 326 (1975)].
- ²¹K. L. Dudko, V. V. Eremenko, and V. M. Fridman, *Zh. Eksp. Teor. Fiz.* **68**, 2315 (1975) [*Sov. Phys. JETP* **41**, 1157 (1975)].
- ²²C. G. Garret, *J. Chem. Phys.* **19**, 1151 (1951).
- ²³S. Katsura and S. Fujimori, *J. Phys. C: Sol. St. Phys.* **7**, 2506 (1974).
- ²⁴L. I. Belyi, N. F. Kharchenko, and V. V. Eremenko, in: *Proc. 19th All-Union Conf. Low Temp. Phys., Minsk (1976)*.
- ²⁵Yu. G. Litvinenko, V. V. Eremenko, and V. I. Myatlik, *Fiz. Tverd. Tela (Leningrad)* **15**, 1284 (1973) [*Sov. Phys. Solid State* **15**, 871 (1973)].
- ²⁶V. S. Borovikov, N. É. Kaner, Yu. G. Litvinenko, A. M. Fridman, and V. V. Shapiro, *Zh. Eksp. Teor. Fiz.* **80**, 1586 (1981) [*Sov. Phys. JETP* **53**, 816 (1981)].
- ²⁷N. F. Kharchenko and L. I. Belyi, *Izv. AN SSSR Ser. Fiz.* **36**, 1230 (1972).
- ²⁸L. I. Belyi, Candidate's Dissertation, FTINT AN Ukr. SSR, Khar'kov (1982).
- ²⁹J. H. Van Vleck and V. V. Pennay, *Phil. Mag.* **17**, 961 (1934).
- ³⁰J. M. Ziman, *Proc. Phys. Soc.* **64A**, 1108 (1951).
- ³¹I. Ono, *J. Phys. Soc. Jpn.* **40**, 213 (1976).
- ³²I. N. Kalinkina, *Zh. Eksp. Teor. Fiz.* **43**, 2028 (1962) [*Sov. Phys. JETP* **16**, 1432 (1962)].
- ³³R. M. Horurech, M. Luban, and S. Shtrikman, *Phys. Lett.* **55A**, 269 (1975).
- ³⁴Yu. A. Izyumov and V. N. Syromyatnikov, *Fazovye Perekhody i Simmetriya Kristallov (Phase Transitions and Crystal Symmetry)*, Nauka, Moscow (1984).
- ³⁵J. Smith and J. M. Yeomas, *J. Phys. C: Sol. St. Phys.* **15**, L1053 (1982).

Translated by A. Mason